Numerical prediction of thermal weakening effects on granite rock

Timo Saksala
Faculty of Built Environment, Tampere University, Tampere, Finland

ABSTRACT: This paper presents a numerical method to predict the temperature weakening effects on granite rock. Thermally induced cracking is modelled in the continuum sense by using a damage-viscoplasticity model based on the rounded Rankine surface. The governing thermo-mechanical problem is solved with an explicit staggered method. Rock heterogeneity is described as random clusters of finite elements assigned with the constituent mineral, here Quartz, Feldspar, and Biotite, material properties. The temperature dependence of the minerals is accounted for up to 800 °C, i.e. well beyond the Curie point (573 °C) of Quartz. The simulations demonstrate that the present approach can accurately predict the experimental weakening effects on the rock strength and stiffness as well as the macroscopic failure modes in tension. Moreover, it does so in a noncircular way, i.e. not using the laboratory data on rock strength as an input data in the constitutive description.

Keywords: Thermal weakening, Rock strength, Granite, Thermo-mechanical problem.

1 INTRODUCTION

High temperature has a detrimental effect on rock strength and stiffness (e.g. Wang & Konietzky 2019; and Toifl et al. 2017). The mechanism behind the thermal weakening under slow uniform heating, i.e., with negligible thermal gradients, can be traced to thermal cracking due to rock heterogeneity. More specifically, the mismatch of the elastic constants and thermal expansion coefficients of different mineral phases induces thermal stresses, which in turn cause cracking. Rocks with Quartz are especially prone to thermal cracking due to its highly nonlinear behavior upon approaching the α-β-transition at 573 °C.

Numerical prediction of thermal effects in rocks is an important topic in rock engineering. Saksala (2022) modelled the thermal weakening effects in granite rock under uniaxial compression and tension by assuming that only the thermal expansion of Quartz phase is (linearly) temperature dependent. This simplified approach successfully predicted the granite strength and stiffness degradation, as well as the 3D failure modes, up to 500 °C. However, deviations from the experimental data occurred at 700 °C, i.e., beyond the α-β-transition. This was clearly due to the simplifying assumption of linear temperature dependence, which is not valid for Quartz mineral. The

purpose of the present paper is to mend this shortcoming by properly accounting for the nonlinear temperature dependence of Quartz thermal and elasticity properties. However, only tension tests are considered in the present study.

2 ROCK NUMERICAL DESCRIPTION

2.1 Rock failure model

The granite rock is modelled as a damaging viscoplastic isotropic and heterogeneous material consisting of Quartz, Feldspar and Biotite mineral phases. The stress states leading to inelastic strain and damage are indicated by the Modified Rankine (MR) criterion, which, along with other model components, is written as:

$$f_{\mathrm{MR}}(\boldsymbol{\sigma},\dot{\lambda}_{\mathrm{MR}}) = \sqrt{\sum_{i=1}^{3}\langle\sigma_i\rangle^2} - (\sigma_{\mathrm{t0}} + s_{\mathrm{MR}}\dot{\lambda}_{\mathrm{MR}}) \tag{1}$$

$$\dot{\boldsymbol{\varepsilon}}_{\mathrm{vp}} = \dot{\lambda}_{\mathrm{MR}}\frac{\partial f_{\mathrm{MR}}}{\partial\boldsymbol{\sigma}}, \omega_{\mathrm{t}} = A_{\mathrm{t}}\left(1-\exp\left(-\beta_{\mathrm{t}}\varepsilon_{\mathrm{eqvt}}^{\mathrm{vp}}\right)\right), \dot{\varepsilon}_{\mathrm{eqvt}}^{\mathrm{vp}} = \sqrt{\sum_{k=1}^{3}\langle\dot{\varepsilon}_{\mathrm{vp},k}\rangle} \tag{2}$$

$$\boldsymbol{\sigma} = (1-\omega_{\mathrm{t}})\bar{\boldsymbol{\sigma}}, \qquad \bar{\boldsymbol{\sigma}} = \mathbf{E}(\theta):\left(\boldsymbol{\varepsilon}-\boldsymbol{\varepsilon}_{\mathrm{vp}}-\boldsymbol{\varepsilon}_{\theta}\right), \qquad \boldsymbol{\varepsilon}_{\theta} = \alpha\Delta\theta\mathbf{I} \tag{3}$$

where σ_i is the ith principal stress of the stress tensor $\boldsymbol{\sigma}$ with the positive parts obtained through Macauley brackets in the MR criterion (1). Moreover, the rest of the symbols are: σ_{t0} is the static tensile strength to which the rate dependent term consisting of the viscosity modulus s_{MR} and the viscoplastic multiplier $\dot{\lambda}_{\mathrm{MR}}$ is added; $\dot{\boldsymbol{\varepsilon}}_{\mathrm{vp}}$ is the rate of viscoplastic strain $\boldsymbol{\varepsilon}_{\mathrm{vp}}$; ω_{t} is the tensile damage variable driven by the equivalent viscoplastic strain $\varepsilon_{\mathrm{eqvt}}^{\mathrm{vp}}$ defined by the rates (increments actually) principal viscoplastic strains $\dot{\varepsilon}_{\mathrm{vp},k}$; A_{t} and $\beta_t = \sigma_{\mathrm{t0}}h_e/G_{\mathrm{Ic}}$ are parameters controlling the final value and the rate of softening with the latter being defined a characteristic length of a finite element and the mode I specific fracture energy G_{Ic}; $\mathbf{E}$ is the elasticity tensor depending on temperature θ; $\boldsymbol{\varepsilon}$ is the total strain. Equation (3) is the nominal-effective stress relation with the constitutive law written under the small deformation assumption. Finally, thermal strain $\boldsymbol{\varepsilon}_{\theta}$ depends linearly on the thermal expansion coefficient α and temperature change $\Delta\theta$. These equations are augmented by the consistency conditions ($f_{\mathrm{MR}} \le 0, \dot{\lambda}_{\mathrm{MR}} \ge 0, \dot{\lambda}_{\mathrm{MR}}f_{\mathrm{MR}} = 0$) and solved at the material (Gauss) point with a standard stress return mapping algorithm.

2.2 Governing thermo-mechanical finite element discretized equations

The finite element discretized thermo-mechanical problem, which can be derived by standard steps using the principle of virtual work, reads:

$$\mathbf{C}_{\theta}(\boldsymbol{\theta})\dot{\boldsymbol{\theta}}_t + \mathbf{f}_{\mathrm{int},t}^{\theta}(\boldsymbol{\theta}_t,\omega_t) = \mathbf{f}_{\theta,t} \;\;\&\;\; \mathbf{M}\ddot{\mathbf{u}}_t + \mathbf{f}_{\mathrm{int},t}(\mathbf{u}_t,\dot{\mathbf{u}}_t,\boldsymbol{\theta}_t) = \mathbf{f}_{\mathrm{ext},t} \tag{4}$$

$$\mathbf{f}_{\mathrm{int}} = \mathbf{A}_{\mathrm{e}=1}^{\mathrm{N_e}}\int_{V_{\mathrm{e}}}\mathbf{B}_{\mathrm{e}}^{\mathrm{T}}\,\boldsymbol{\sigma}_{\mathrm{e}}(\mathbf{u}_t,\dot{\mathbf{u}}_t,\boldsymbol{\theta}_t,\omega_t)\mathrm{d}V, \quad \mathbf{M} = \mathbf{A}_{\mathrm{e}=1}^{\mathrm{N_e}}\int_{V_{\mathrm{e}}}\rho{\mathbf{N}_{\mathrm{e}}}^{\mathrm{T}}\mathbf{N}_{\mathrm{e}}\,\mathrm{d}V \tag{5}$$

$$\mathbf{C}_{\theta} = \mathbf{A}_{\mathrm{e}=1}^{\mathrm{N_e}}\int_{V_{\mathrm{e}}}\rho c(\theta)\mathbf{N}_{\theta}^{\mathrm{e,T}}\mathbf{N}_{\theta}^{\mathrm{e}}\mathrm{d}V, \quad \mathbf{f}_{\mathrm{int},t}^{\theta} = \mathbf{A}_{\mathrm{e}=1}^{\mathrm{N_e}}\int_{V_{\mathrm{e}}}(1-\omega_t)k(\theta)\mathbf{B}_{\theta}^{\mathrm{e,T}}\boldsymbol{\theta}_t^{\mathrm{e}}\mathrm{d}V \tag{6}$$

$$\mathbf{f}_\theta = \mathbf{A}_{e=1}^{N_e} \int_{V_e} Q_{\text{int}} \mathbf{N}_\theta^{e,T} \, dV \tag{7}$$

where the symbols are as follows: $\mathbf{M}$ is the consistent mass matrix (to be lumped by the row sum technique) with density ρ; $\mathbf{C}$ is thermal capacity matrix (to be lumped by the row sum technique) where the heat capacity c depends on temperature; $\mathbf{f}_{\text{int},t}^{\theta}$ is the internal thermal force vector depending explicitly on damage and implicitly on temperature, via conductance k; $\mathbf{f}_{\text{ext}}$ is the external force vector; $\mathbf{f}_{\text{int}}$ is the internal mechanical force vector defined in (5); $\mathbf{f}_\theta$ is the vector of thermal loading with Q_{int} being the volumetric heating magnitude (flux); $\mathbf{A}$ is the standard finite element assembly operator; $\mathbf{B}_e$ is the kinematic matrix (mapping the nodal displacement into element strains); $\boldsymbol{\theta}$ is the nodal temperature vector; $\mathbf{N}_\theta$ and $\mathbf{N}_e$ are the temperature and displacement interpolation matrices (same interpolation functions are used in both); $\mathbf{B}_\theta$ is the gradient of $\mathbf{N}_\theta$. The system (4) is solved by explicit time stepping in a staggered manner. Mass scaling is used for the mechanical part of the problem to increase the critical time step of explicit integrator. For more details, see Saksala (2022).

2.3 Temperature dependence of rock material properties

Granite material properties depend strongly on temperature, especially those of Quartz. However, it should be strongly emphasized that when predicting the thermal weakening effect by numerical modelling, the temperature dependence of the strength cannot be fed into the model as an input data – that would beg the question, i.e., it would be circular reasoning. Moreover, it is not even legitimate to do so because the strength (tensile and compressive) is measured for a laboratory size specimen, not at the material point level where the constitutive equation is written and implemented. Therefore, only the elastic constants and thermal properties are temperature dependent here.

The laboratory data provided by Wang & Konietzky (2019) and Toifl et al. (2017) is used here. Figure 1 shows the temperature dependencies of the rock material properties implemented in the present material model. Linear interpolation is applied between the datapoints.

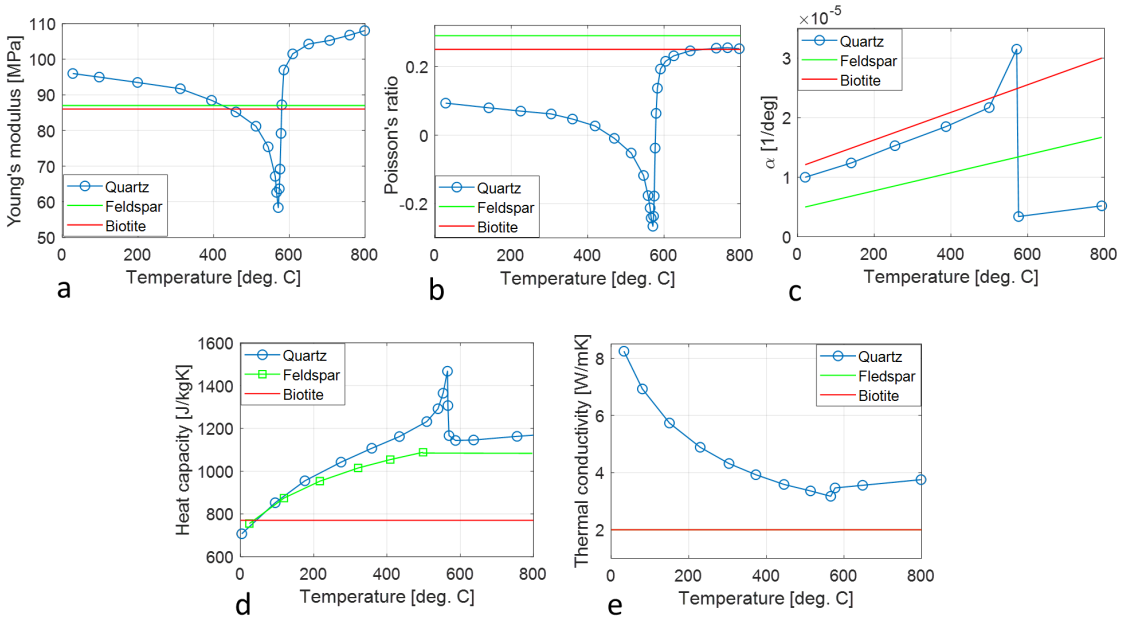

Figure 1. Temperature dependence of Young's modulus (a), Poisson's ratio (b), thermal expansion (c), heat capacity (d), and thermal conductivity (e) (the datapoints in Wang & Konietzky (2019) and Toifl et al. (2017) are reproduced by a plot digitizer software).

As observed in Figure 1, Quartz is the deviant mineral while Feldspars and Biotite (Micas in general) can be taken mostly independent of temperature within this range for these properties. Moreover, it is noted that the thermal expansion coefficient data for Quartz in Figure 1c is for Granite by Heuze (1983). The true temperature dependence of Quartz is not used here due to its extremely anomalous behavior: Upon reaching the Curie point 573 °C, where the α-β-transition takes place, the thermal expansion coefficient of Quartz reaches 13 times the value it has at 25 °C (Wang & Konietzky 2019). When the true behavior was implemented, the results to be presented in the next section, were not realistic. Furthermore, the latent heat related to the α-β phase change is -9.8 J/g (Carpenter et al. 1998) while the latent heat of Granite in melting is 420 J/g. Therefore, the Quartz phase change can be ignored from the computational point of view. The rest of the material properties and model parameters for simulations are given in Table 1.

Table 1. Material properties and model parameters for simulations.

Parameter / Mineral	Quartz	Feldspar	Biotite
E [GPa]	96	87	86
ν	0.093	0.29	0.25
σ_{t0} [MPa]	14	8	7
ρ [kg/m^3]	2650	2620	3050
G_{Ic} [J/m^2]	100	100	70
α_0 [1/K]	1.0E-5	0.5E-5	1.2E-5
k_0 [W/mK]	707	754	77
c_0 [J/kgK]	8.2	2.0	2.0
A_t	0.98	0.98	0.98
s_{RM} [MPa·s]	0.01	0.01	0.01
f [%]	25	65	10

The parameters in Table 1 having subscript "0" are given at the room temperature. Moreover, the viscosity values given are small enough not to cause any strain rate effects in the low-rate tension tests presented in the next section. Finally, the percentages in the last row in Table 1 mean the percentage of the mineral in the numerical rock.

3 NUMERICAL SIMULATIONS

3.1 Numerical heating of rock samples

Following Saksala (2022), uniform heating up to 300 °C, 500 °C and 700 °C is carried out on the numerical rock samples. As mentioned above, mass scaling is applied here to increase the critical time step of the explicit time stepping. This is enabled by the non-inertial nature of slow oven heating. In addition, volumetric heating is applied with Q_{int} = 1E10 W/m^3 (Equation (7)) at each node of mesh to secure a homogenous temperature field in the rock sample. The rock mineral mesotexture is described as random clusters of finite elements.

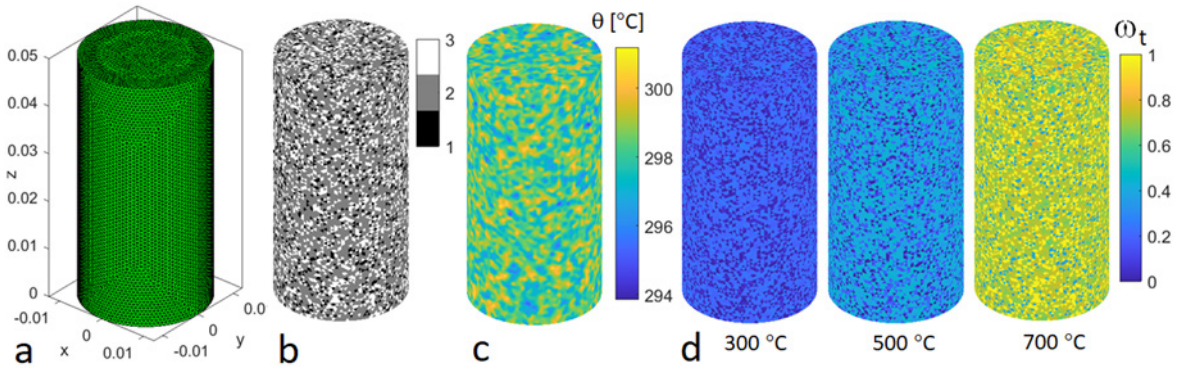

Figure 2. Simulation results for thermal treatment: (a) Finite element mesh with 488898 linear tetrahedrons; (b) Rock mineral texture (Quartz = 3, Feldspar = 2, Biotite = 1); (c) Temperature distribution at the end of heating to 300 °C; (d) Tensile damage distributions at the end of heat treatments.

Figure 2 shows the simulation results at the end of heating process. Due to the heterogeneous material description and the extremely short heating time of ~0.1 s, the temperature distribution is not uniform but varies from 294 to 301 °C, as seen in Figure 2c. The magnitude of damage is quite mild below the α-β-transition. Next, the uniaxial tension test is carried out on the intact and heat-treated samples.

3.2 Numerical tension tests

Uniaxial tension tests are performed on an intact numerical rock and the heat-treated, cooled down samples. A velocity of 0.05 m/s, which corresponds to a strain rate of 1 s^{-1}, is applied at the top surface of the numerical sample. The results are shown in Figure 3.

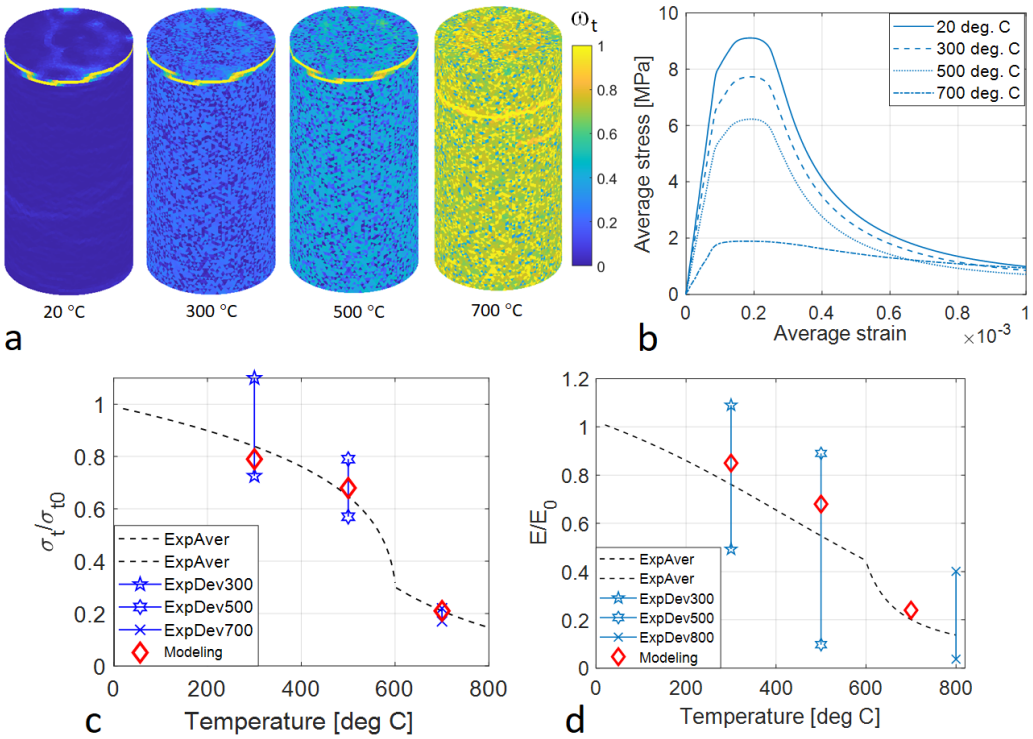

Figure 3. Simulation results for tension tests: (a) Failure modes at different temperatures in terms of tensile damage patterns; (b) Average stress-strain curves; (c), (d) Predicted normalized tensile strengths at different temperatures including mean fitted curve and the experimental data scatters for tensile strength and Young's modulus measured from the curves in Figure 3c (data reproduced from Wang & Konietzky (2019)).

All the numerical samples have failed in the experimental transverse splitting mode with a single failure plane (Figure 3a). The corresponding stress-strain curves (Figure 3b) display a mild pre-peak nonlinearity followed by exponential softening. The predicted tensile strengths are within the experimental bounds, even at 700 °C, which was not the case in Saksala (2022). Finally, the predicted degradation of Young's modulus, measured from the curves in Figure 3c, is also in agreement with the experiments, as can be observed in Figure 3d.

4 CONCLUSIONS

Thermally induced degradation of Granite under uniform slow heating was numerically studied by the continuum approach based on a damage-viscoplasticity model. The peculiar behavior of Quartz mineral was properly modelled by taking laboratory data for the elasticity constants and thermal properties into account for a wide range of temperatures. With this approach, Granite failure modes, as well as the strength and stiffness degradation in tension can be accurately predicted up to 800 °C, i.e. well beyond the α-β-transition of Quartz, as was demonstrated in this paper. It is emphasized that the present approach does not use the measured data for the tensile strength temperature dependence as a model input. It, therefore, predicts the strength degradation in a noncircular way.

REFERENCES

Carpenter, M.A., Salje, E.K.H., Graeme-Barber, A., Wruck, B., Dove, M.T., Knight, K.S. 1998. Calibration of excess thermodynamic properties and elastic constant variations associated with the α-β phase transition in quartz. *American Mineralogist* 83, pp. 2-22.

Heuze, F.E. 1983. High-temperature mechanical, physical and thermal properties of granitic rocks—a review. *International journal of rock mechanics and mining sciences & geomechanics abstracts* 20 (1), pp. 3-10.

Saksala, T. 2022. 3D numerical prediction of thermal weakening effects on granite. *International Journal for Numerical and Analytical Methods in Geomechanics* 46, pp. 2770-2791.

Toifl, M., Hartlieb, P., Meisels, R., Antretter, T., Kuchar, F. 2017. Numerical study of the influence of irradiation parameters on the microwave-induced stresses in granite. *Mineral Engineering* 103-104, pp. 78–92.

Wang, F. & Konietzky, H. 2019. Thermo-Mechanical Properties of Granite at Elevated Temperatures. and Numerical Simulation of Thermal Cracking. *Rock Mechanics and Rock Engineering* 52, pp. 3737-3755.